Neuromodulation: Technology at the Neural Interface

Received: February 22, 2022 Revised: July 1, 2022 Accepted: July 9, 2022

https://doi.org/10.1016/j.neurom.2022.07.006

Bioheat Model of Spinal Column Heating During High-Density Spinal Cord Stimulation

Adantchede L. Zannou, BE[1]; Niranjan Khadka, PhD[2]; Marom Bikson, PhD[1]

ABSTRACT

Introduction: High-density (HD) spinal cord stimulation (SCS) delivers higher charge per time by increasing frequency and/or pulse duration, thus increasing stimulation energy. Previously, through phantom studies and computational modeling, we demonstrated that stimulation energy drives spinal tissue heating during kHz SCS. In this study, we predicted temperature increases in the spinal cord by HD SCS, the first step in considering the potential impact of heating on clinical outcomes.

Materials and Methods: We adapted a high-resolution computer-aided design–derived spinal cord model, both with and without a lead encapsulation layer, and applied bioheat transfer finite element method multiphysics to predict temperature increases during SCS. We simulated HD SCS using a commercial SCS lead (eight contacts) with clinically relevant intensities (voltage-controlled: 0.5–7 V_{rms}) and electrode configuration (proximal bipolar, distal bipolar, guarded tripolar [+−+], and guarded quadripolar [+−−+]). Results were compared with the conventional and 10-kHz SCS (current-controlled).

Results: HD SCS waveform energy (reflecting charge per second) governs joule heating in the spinal tissues, increasing temperature supralinearly with stimulation root mean square. Electrode configuration and tissue properties (an encapsulation layer) influence peak tissue temperature increase—but in a manner distinct for voltage-controlled (HD SCS) compared with current-controlled (conventional/10-kHz SCS) stimulation. Therefore, depending on conditions, HD SCS could produce heating greater than that of 10-kHz SCS. For example, with an encapsulation layer, using guarded tripolar configuration (500-Hz, 250-μs pulse width, 5-V_{peak} HD SCS), the peak temperature increases were 0.36 °C at the spinal cord and 1.78 °C in the epidural space.

Conclusions: As a direct consequence of the higher charge, HD SCS increases tissue heating; voltage-controlled stimulation introduces special dependencies on electrode configuration and lead encapsulation (reflected in impedance). If validated with an in vivo measurement as a possible mechanism of action of SCS, bioheat models of HD SCS serve as tools for programming optimization.

Keywords: Bioheat modeling, electrode encapsulation, electrodes configuration, high-density spinal cord stimulation, voltage-controlled stimulation

Conflict of Interest: The City University of New York has intellectual property (IP) on neuro-stimulation systems and methods with authors Niranjan Khadka and Marom Bikson as inventors. Niranjan Khadka consults for Ybrain Inc. Marom Bikson has equity in Soterix Medical Inc. Marom Bikson consults, received grants, assigned inventions, and/or serves on the SAB of SafeToddles, Boston Scientific, GlaxoSmithKline, Biovisics, Mecta, Lumenis, Halo Neuroscience, Google-X, i-Lumen, Humm, Allergan (Abbvie), and Apple. Adantchede L. Zannou reported no conflict of interest.

INTRODUCTION

To optimize pain control and patient acceptance, novel approaches for spinal cord stimulation (SCS) programming are being developed. High-density (HD) SCS delivers higher charge per second by increasing duty cycle (increasing frequency and/or pulse width).[1–4] Duty cycles of HD SCS are 9% to 50%,[1,5–7] compared with 2% to 4% for conventional SCS and 40% to 80% for kHz SCS.[1,2,8,9] Charge per second increases with duty cycle times the stimulation peak intensity. It is noteworthy that when only one pulse phase is used in calculation (ie, counting pulses of one phase and disregarding pulses of the other phase), these reported duty cycles are halved. Stimulation energy increases with duty cycle times the square of intensity.[10] Clinically, HD SCS allows pain relief without paresthesia through administering subthreshold intensity; nonetheless, charge per second and energy applied are relatively high compared with conventional SCS.[4,6,10,11]

Address correspondence to: Adantchede L. Zannou, BE, Department of Biomedical Engineering, The City College of New York, Center for Discovery & Innovation, 85 St Nicholas Terrace, Room 3.368, New York, NY 10031, USA. Email: azannou00@citymail.cuny.edu

[1] Department of Biomedical Engineering, The City College of New York, New York, NY, USA; and
[2] Department of Psychiatry, Division of Neuropsychiatry and Neuromodulation, Massachusetts General Hospital, Harvard Medical School, Boston, MA, USA

For more information on author guidelines, an explanation of our peer review process, and conflict of interest informed consent policies, please see the journal's Guide for Authors.

Source(s) of financial support: This study was partially funded by grants to Marom Bikson from Harold Shames and the National Institutes of Health (NIH): NIH-National Institute on Drug Abuse (NIDA) UG3DA048502, NIH-National Institute of General Medical Sciences (NIGMS) T34GM137858, NIH-National Institute of Neurological Disorders and Stroke (NINDS) 1R01NS112996, NIH-NINDS 1R01NS101362, NIH-National Institute of Mental Health (NIMH) 1R01MH111896, and NIH-NINDS 1R01NS095123.

We previously showed using phantom measurements and bioheat finite element method (FEM) computational models that increased SCS energy—whether by frequency and pulse duration (duty cycle) or intensity—contributes to increasing spinal tissue temperature through joule.[8,9] In this study, we simulate spinal tissue heating by HD SCS, including consideration of the impact of voltage-controlled stimulation, multipolar guarded electrode configurations, and an encapsulation layer (from scar tissue formation around the lead[12,13]). We predict that the high charge per time characteristic of HD SCS increases spinal tissue heating, and that voltage-controlled stimulation introduces special sensitivity to electrode configuration and lead encapsulation.

MATERIALS AND METHODS

We adapted a computer-aided design (CAD) model of the of lower thoracic (T8–T12) spinal cord with seven tissue compartments, including the vertebrae, intervertebral disc, soft tissues, epidural fat, dura, cerebrospinal fluid (CSF), and spinal cord (white matter and gray matter combined) in SolidWorks 2016 (Dassault Systemes Americas Corp, Waltham, MA) (Fig. 1). A simulated Medtronic Vectris SureScan HD SCS lead (1x8 Compact (977A2), Medtronic, Minneapolis, MN; electrode diameter: 1.3 mm; electrode length: 3.0 mm; edge-to-edge interelectrode spacing: 4 mm) was positioned in the epidural fat (approximately 5.1 mm away from the dorsal surface of the spinal cord, along the mediolateral midline of the spine). We modeled only a single lead, although SCS also may be applied with multiple leads. The dimensions of the individual tissues, modeled here as an isotropic homogeneous volume conductors, were based on our previous studies.[8,9] The entire CAD model assembly was then manually segmented and meshed into a finer mesh using a built-in voxel-based adaptive meshing algorithm of Simpleware ScanIP (Synopsys Inc, Mountain View, CA). Mesh density was refined until additional model refinement produced a <1% difference in peak temperature change and peak electric field. The resulting mesh consisted of >13.5 million tetrahedral elements. The final FEM model was later imported and computationally solved in COMSOL (COMSOL Multiphysics, Boston, MA).

During HD SCS, joule heating is produced by an electrical current flow through the tissue. This thermal energy source was modeled as $\sigma|\nabla V|^2$, where V (Volts) is an induced local potential by stimulation and σ (S m^{-1}) is the electrical conductivity of the tissue. We assumed a quasi-static electrical conduction model, which allowed us to apply Laplace's equation to compute the electric potential V (Volts) as follows[14–16]:

$$\nabla \cdot [\sigma \nabla V] = 0 \tag{1}$$

Consequently, a constant voltage/current was administered corresponding to the stimulation root mean square (RMS) (at the anode, with the cathode grounded). Based on our previous analysis, providing an electrode boundary condition with the appropriate constant RMS value correctly predicts resulting temperature change.[8,9,15,17] RMS SCS intensities were calculated based on corresponding peak intensities and stimulation waveform parameters, as previously derived.[8,9,15,17] The relationship between stimulation RMS and duty cycle, DC, is shown in Equation (2)

$$X_{RMS} = X_{Peak}\sqrt{DC} \tag{2}$$

where $DC = \frac{Pulse\ Width}{Pulse\ Duration}$, X_{Peak} is the peak bipolar stimulation intensity, and X_{RMS} is the corresponding RMS value for current-controlled or voltage-controlled stimulation.

We coupled joule heating during SCS [Equation (1)] and solved the Pennes bioheat transfer equation to approximate the temperature distribution throughout a perfused tissue as

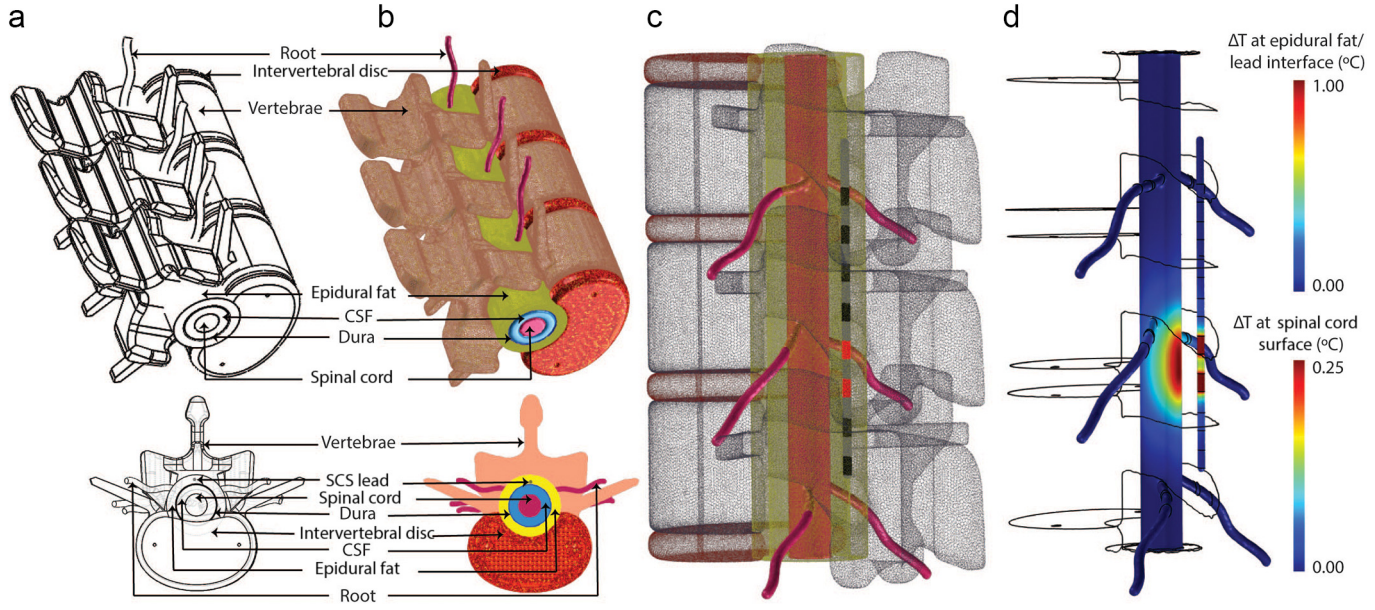

Figure 1. SCS FEM bioheat model design. a. CAD–derived human spinal cord anatomy of the lower thoracic spine (T8–T10) with seven segmented spinal tissue compartments and an epidurally implanted commercial eight contact SCS lead. b and c. Different views of the meshed spinal cord FEM model. d. Predicted maximum temperature increase at the epidural space (electrode surface) and spinal cord. [Color figure can be viewed at www.neuromodulationjournal.org]

Table 1. Biophysical and Thermo-Electrical Properties of the Modeled Biological Tissues.

Spinal tissues	Soft tissue	Vertebrae	IV disc	Epidural fat	Dura	CSF	Spinal cord	Encapsulation
Conductivity, σ (S m^{-1})	0.004	0.04	0.6	0.04	0.368	1.77	0.1432	0.13
Thermal conductivity, κ (W m^{-1} k^{-1})	0.47	0.32	0.49	0.21	0.44	0.57	0.51	0.21
Blood density, ρ_b (kg m^{-3})	1057	1057	0	1057	1057	0	1057	1057
Specific heat capacity of blood, C_b (J kg^{-1} K^{-1})	3600	3600	0	3600	3600	0	3600	3600
Blood perfusion rate, ω_b (s^{-1})	0.00009	0.00048	0	0.00008	0.009	0	0.009	0.00008
Metabolic heat generation rate, Q_{met} (W m^{-3})	368	26.1	0	302	15,575	0	15,575	302

In avascular tissues, blood properties and Q_{met} are set to zero.
IV, intervertebral.

$$\rho C_p \frac{\partial T}{\partial t} = \nabla.(\kappa \nabla T) - \rho_b C_b \omega_b (T - T_b) + Q_{met} + \sigma |\nabla V|^2 \quad (3)$$

where ρ,ρ_b,C_p,T_b,κ,ω_b,C_b, and Q_{met} are the spinal tissue density (kg m^{-3}), blood density, specific heat capacity of the spinal tissues (J kg^{-1} K^{-1}), core/blood temperature (K), thermal conductivity of the spinal tissues (W m^{-1} K^{-1}), blood perfusion rate (s^{-1}), blood specific heat capacity, and metabolic heat generation rate (W m^{-3}), respectively.[15,18] We solved the model under steady state assumption ($\frac{\partial T}{\partial t} = 0$).

The biophysical and thermo-electrical properties of biological tissues were based on previous studies.[6,8,9,19–23] The assigned properties for different spinal tissues are listed in Table 1.

The thermo-electric properties of the SCS lead were given as platinum/iridium contact ($\sigma = 4 \times 10^6$ S m^{-1}; $\kappa = 31$ W m^{-1} K^{-1}) and polyurethane interelectrode gap ($\sigma = 2 \times 10^{-6}$ S m^{-1}; $\kappa = 0.026$ W m^{-1} K^{-1}). The role of scar tissue formation (encapsulation), an inflammatory response after an SCS implant, has been previously studied.[12,24] The resistivity of the encapsulation tissue alters the electric field generation and distribution around chronically implanted electrodes.[22,23] Here, we simulated and contrasted the effect of an encapsulation layer on spinal tissue heating for the undermentioned stimulation conditions. Thermo-electric properties of the lead encapsulation layer were assigned as indicted in Table 1.[12,22,23,25,26]

In studies comparing HD SCS, conventional SCS, and 10-kHz SCS, a proximal bipolar configuration was simulated by energizing the third electrode of the stimulation lead or E3 (cathode) and E4 (anode). Additional HD SCS electrode configurations were distal bipolar (E1 [cathode], E8 [anode]), guarded quadripolar (E3 [anode], E4 [cathode], E5 [cathode], E6 [anode]), and guarded tripolar (E4 [anode], E5 [cathode], E6 [anode]). The remaining external boundaries of the spinal cord and surrounding tissues were electrically insulated.[15,17,24] For thermal boundary condition, the temperature at the outer boundaries of the model was fixed at the core body temperature (37 °C), assuming no convective heat loss to the ambient temperature, no convective gradients across the spinal surrounding tissues, and no SCS-induced heating at the model boundaries. The initial temperature of the tissues was set to the core body temperature.[15,17,24] To ensure model boundaries and mesh resolution did not affect the results, we confirmed 1) a <0.01 °C increase in temperature at the model boundaries when SCS was activated; 2) a <0.001% increase in current density at the model boundaries during SCS; and 3) a <5% temperature increase when relative tolerance was decreased by 100×. It should be noted that monopolar stimulation was not simulated in this work; therefore, the outer boundaries were not grounded.

Using clinically relevant HD SCS intensities (0.5–7 V_{peak})[1,6,10] and electrode configurations (proximal bipolar, distal bipolar, guarded tripolar [+−+], and guarded quadripolar [+−−+]), we predicted the maximum temperature increase by a commercial SCS lead, both with and without a lead encapsulation layer (Fig. 1). Wherever stated, the RMS SCS intensities were calculated based on corresponding peak intensities and stimulation waveform parameters, as previously derived.[8,9] For stimulation RMS value calculation purposes, we assumed that all SCS systems waveform outputs were biphasic symmetric. The maximum temperature increases by voltage-controlled HD SCS (frequency = 500 Hz, pulse width = 250 µs, V_{peak} = 5 V) were compared with current-controlled conventional SCS (frequency = 50 Hz, pulse width = 200 µs, I_{peak} = 3.5 mA)[1,2,27] and 10-kHz SCS (frequency = 10 kHz, pulse width = 30 µs, I_{peak} = 3.5 mA)[2,8,9,28] for a proximal bipolar electrode configuration, both with and without lead encapsulation conditions. It should be noted that for each SCS approach, we evaluated clinically applicable (but relatively high) stimulation doses.[1,3,4,7,9,11,29] In a separate analysis, we simulated the sensitivity of maximum temperature increase with various RMS intensities (Table 2).

RESULTS

We implemented a CAD–derived FEM bioheat computational model of HD SCS to predict local spinal tissue heating using a commercial eight-contact SCS lead at various clinically relevant intensities (voltage-controlled: 0.5–7 V_{rms}), electrode configurations (proximal bipolar, distal bipolar, guarded tripolar [+−+], and guarded quadripolar [+−−+]), and under encapsulation or non-encapsulation conditions. These results were compared with predictions for current-controlled conventional SCS and 10-kHz SCS.

We first considered maximum temperature increases at both the lead surface (epidural space) and spinal cord surface by conventional SCS, HD SCS, and 10-kHz SCS, all using proximal bipolar electrodes (Fig. 2). For each SCS approach, we evaluated clinically typical (but relatively high) stimulation doses (conventional: 50 Hz, 200 µs 3.5 mA_{peak}; HD SCS: 500 Hz, 250 µs, 5 V_{peak}; 10-kHz SCS: 10 kHz, 30 µs, 3.5 mA_{peak}). HD SCS is voltage-controlled, whereas conventional and 10-kHz SCS are current-controlled. In this series, only a proximal bipolar configuration was considered, and both

Table 2. Sensitivity of HD SCS Intensities (RMS) on Maximum Temperature Increase Across Different Electrode Configurations, Both Without and With Encapsulation Tissue Layer.

A. Nonencapsulated simulation lead

	Proximal		Distal		Guarded + − − +		Guarded + − +	
RMS (V)	Electrode	SC	Electrode	SC	Electrode	SC	Electrode	SC
0.5	0.038	0.000	0.032	0.000	0.039	0.000	0.043	0.000
1.5	0.120	0.009	0.098	0.003	0.130	0.019	0.191	0.023
2.5	0.288	0.061	0.218	0.026	0.303	0.076	0.485	0.075
3.5	0.560	0.120	0.424	0.060	0.597	0.148	0.927	0.163
4	0.694	0.141	0.547	0.081	0.760	0.183	1.203	0.215
5	1.068	0.226	0.841	0.132	1.170	0.291	1.865	0.344
7	2.066	0.451	1.623	0.269	2.270	0.577	3.633	0.683

B. Encapsulated simulation lead

	Proximal		Distal		Guarded + − − +		Guarded + − +	
RMS (V)	Electrode	SC	Electrode	SC	Electrode	SC	Electrode	SC
0.5	0.060	0.002	0.047	0.000	0.058	0.005	0.069	0.005
1.5	0.210	0.038	0.140	0.017	0.222	0.052	0.333	0.061
2.5	0.505	0.127	0.337	0.058	0.551	0.158	0.851	0.175
3.5	0.950	0.250	0.650	0.120	1.103	0.300	1.777	0.357
4	1.232	0.294	0.834	0.155	1.352	0.379	2.165	0.456
5	1.902	0.460	1.283	0.246	2.089	0.592	3.337	0.703
7	3.693	0.895	2.483	0.483	4.053	1.157	6.480	1.380

All ΔT values are in °C. Maximum temperature at the epidural space (electrode) and SC with and without encapsulation increased with RMS intensities, higher with encapsulation layer and guarded tripolar [+−+] electrode configuration. Predicted maximum temperature at the epidural space and spinal cord for different electrode configurations at clinically relevant HD SCS intensities for (A) nonencapsulation stimulation lead and (B) encapsulation stimulation lead. For each RMS stimulation intensity, the corresponding peak voltage assuming 500 Hz, 250 μs is noted.
Electrode, sampled at the electrode/epidural fat interface; SC, sampled at the spinal cord surface.

encapsulation layer absent and present conditions were simulated. For the nonencapsulated lead condition (Fig. 2a), the maximum temperature increase (ΔT) at the spinal cord was 0.003 °C for conventional SCS, 0.12 °C for HD SCS, and 0.32 °C for kHz SCS. For the nonencapsulated lead condition, ΔT at the epidural surface was 0.12 °C for conventional SCS, 0.56 °C for HD SCS, and 1.50 °C for kHz SCS. For the encapsulated lead condition (Fig. 2b), ΔT at the spinal cord was 0.0025 °C for conventional SCS, 0.25 °C for HD SCS, and 0.16 °C for kHz SCS. ΔT at the epidural surface for the encapsulated lead condition was 0.01 °C for conventional SCS, 1.00 °C for HD SCS, and 0.8 °C for kHz SCS. Therefore, the addition of the lead encapsulation layer increased the temperature for the HD SCS while decreasing the temperature for the conventional and 10-kHz SCS cases. Using proximal bipolar electrodes, the maximum spinal cord temperature increase of 0.25 °C was predicted for the HD SCS (500 Hz, 250 μs, 5 V_{peak}) condition with encapsulation, whereas the maximum epidural temperature increase of 1.50 °C was predicted for the 10-kHz SCS (10 kHz, 30 μs, 3.5 mA_{peak}) condition without encapsulation.

With computational models, one can assess whether differences in heating between voltage-controlled and current-controlled stimulation reflect a fundamental difference in processes or are interchangeable, provided the applied voltage is adjusted to a target current (or vice versa). The impedance (measured between the simulated electrodes) encountered by the HD SCS lead between the proximal bipolar electrodes was 2170 Ω without encapsulation layer and 1130 Ω with encapsulation layer (calculated by Ohm's law: I = V / Z). Using these interelectrode impedances and applying Ohm's law, 5-V_{peak} HD SCS corresponds to 2.28 mA_{peak} without encapsulation and to 4.38 mA_{peak} with encapsulation. In control simulations, we confirmed applying these as current-controlled inputs to the respective models, resulting in the same temperature increases as voltage-controlled (not shown). Voltage-controlled and current-controlled are thus interchangeable to the extent lead impedance is accounted for. For each voltage-controlled simulation, we report the corresponding equivalent current, and for current-controlled simulation, we report the corresponding voltage across the electrodes (values with asterisks, Figs. 2 and 3).

Focusing on HD SCS (500 Hz, 250 μs, 5 V_{peak}), we next predicted the impact of electrode configuration, both without (Fig. 3a) and with lead encapsulation (Fig. 3b). Without an encapsulation layer, the maximum temperature increases predicted in the epidural space and at the spinal cord surface, respectively, using proximal bipolar electrode configurations were 0.56 °C/0.12 °C, distal bipolar were 0.42 °C /0.06 °C, guarded quadripolar were 0.60 °C/0.15 °C, and guarded tripolar were 0.92 °C/0.16 °C. With an encapsulation layer, the maximum temperature increases predicted in the epidural space and at the spinal cord, respectively, using proximal bipolar electrode configurations were 1.00 °C/0.25 °C, distal bipolar were 0.65 °C/0.12 °C, guarded quadripolar were 1.10 °C/0.30 °C, and guarded tripolar were 1.78 °C/0.36 °C. Therefore, across electrode configurations, the temperature increased by HD SCS (500 Hz, 250 μs, 5 V_{peak}) was maximum for the guarded tripolar

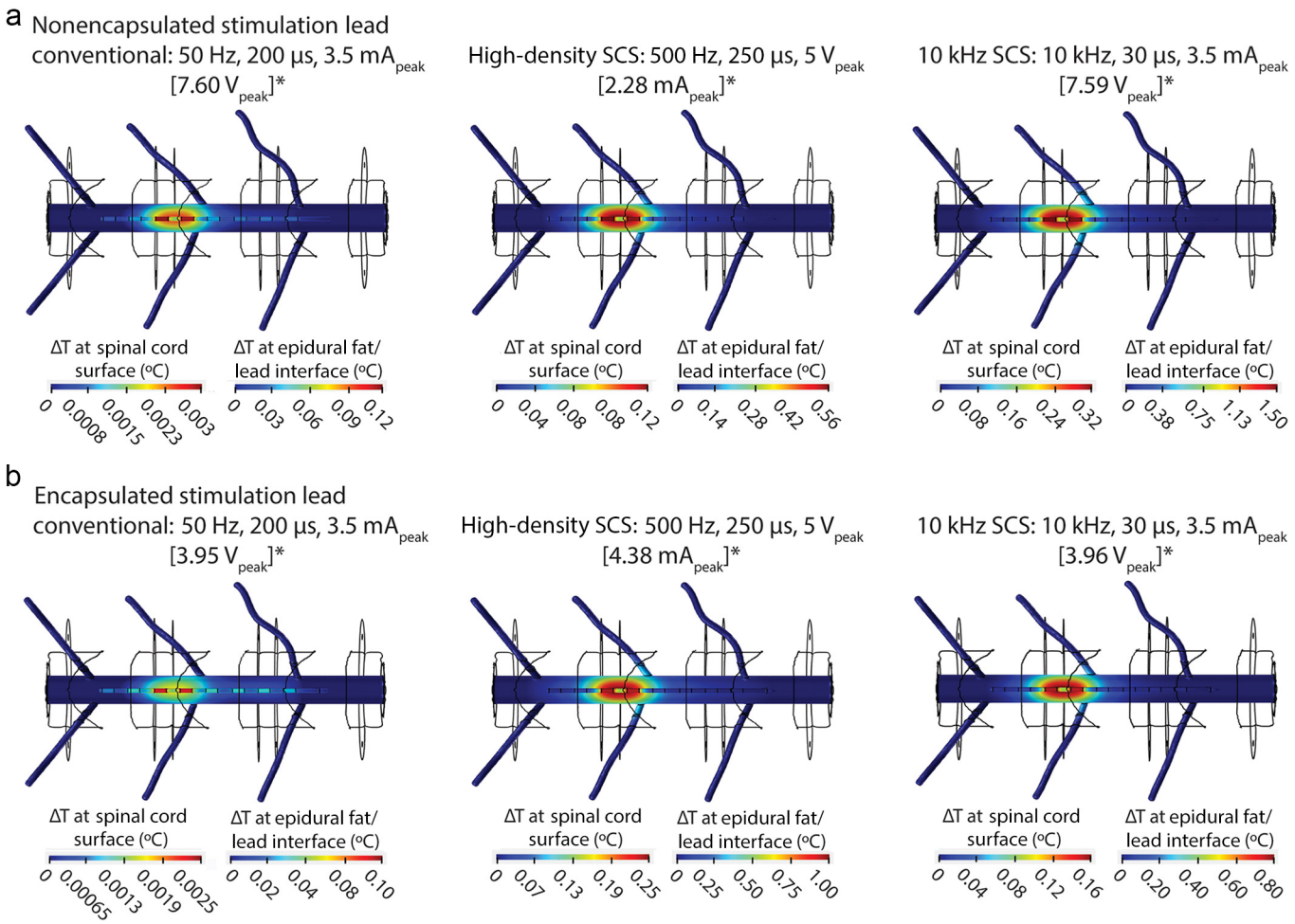

Figure 2. Role of encapsulation on spinal tissue heating during conventional SCS, HD SCS, and 10-kHz SCS using clinically typical stimulation programming and a proximal bipolar electrode configuration. a. For the nonencapsulated SCS lead condition, the maximum temperature increases for the conventional SCS, HD SCS, and 10-kHz SCS were 0.12 °C, 0.56 °C, and 1.50 °C at the epidural fat and 0.003 °C, 0.12 °C, and 0.32 °C at the spinal cord, respectively. b. For the encapsulated SCS lead condition, the maximum temperature increases for the conventional SCS, HD SCS, and 10-kHz SCS were 0.10 °C, 1.00 °C, and 0.80 °C at the epidural space and 0.0025 °C, 0.25 °C, and 0.16 °C at the spinal cord, respectively. *For each voltage-controlled simulation, the corresponding equivalent current is reported. [Color figure can be viewed at www.neuromodulationjournal.org]

configuration—both without (0.16 °C at the spinal cord; 0.92 °C at the epidural space) and with encapsulation (0.36 °C at the spinal cord; 1.78 °C at the epidural space).

The interelectrode impedance (anode[s] to cathode[s]) for each SCS electrode configuration, with/without an encapsulation layer, respectively, were proximal bipolar: 2170 Ω/1130 Ω (as noted earlier), distal bipolar: 2325 Ω/1313 Ω, guarded quadripolar: 1088 Ω/572 Ω, and guarded tripolar: 1580 Ω/822 Ω. Based on these impedances, the resulting current produced in each configuration is reported (values with asterisks, Fig. 3). Each of these impedance values is measured between active electrodes (so are bipolar impedances rather than single-electrode unipolar impedance) and is then consistent with existing clinical data.[1,10,29,30] The ranking of temperature increase within each electrode configuration is predicted by the resulting current.

We previously showed that heating by SCS depends on stimulation RMS, irrespective of specific waveform parameters (frequency, pulse duration, intensity).[9] To predict heating by SCS, the RMS can be calculated and applied to the bioheat model (Equation (2)). The sensitivity of maximum temperature increase at the epidural space and the spinal cord to the stimulation RMS was predicted, across electrode configurations and both without and with encapsulation (Table 2). For any given intensity and electrode configuration, heating was greater with encapsulation than without. The guarded tripolar electrode configuration produced the maximum heating for any given intensity and encapsulation condition.

Having contrasted clinically relevant SCS parameters, we next systematically explained the impact of the encapsulation layer on current-controlled vs voltage-controlled stimulation. To this end, starting with the nonencapsulated layer condition, we simulated the proximal bipolar HD SCS under voltage-controlled (V = 5 V_{peak}; Fig. 4a) and current-controlled, with an applied current value matching that result in the voltage-controlled case without encapsulation (I = 1.61 mA_{peak}; Fig. 4b)—we expected these simulations to produce similar results (as noted earlier). Next, the encapsulation layer was added to the voltage-controlled (Fig. 4c) and current-controlled (Fig. 4c) cases. For voltage-controlled stimulation, the addition of an encapsulation layer slightly decreased the peak electric field (from 5190 V/m to 4790 V/m) and doubled the peak current

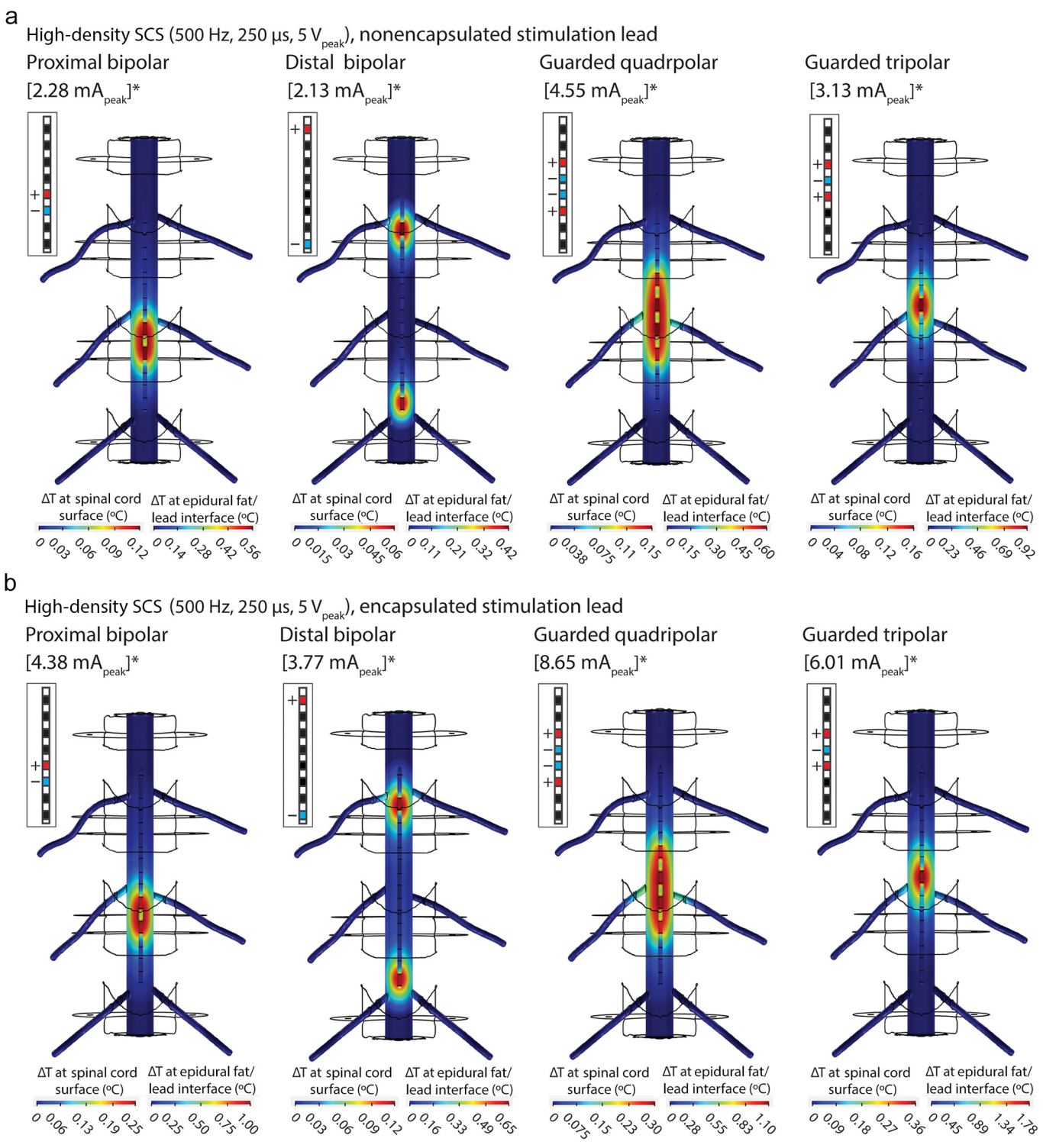

Figure 3. Role of electrode configuration on spinal tissue heating without and with lead encapsulation layer during HD SCS. a. For the nonencapsulated SCS lead condition, the whole volume maximum temperature increases at the epidural space and spinal cord were 0.56 °C and 0.12 °C for proximal bipolar, 0.42 °C and 0.06 °C for distal bipolar, 0.60 °C and 0.015 °C for guarded quadripolar, and 0.92 °C and 0.16 °C for guarded tripolar configuration, respectively. b. For the encapsulated SCS lead condition, the whole volume maximum temperature increases at the epidural space and spinal cord were 1.00 °C and 0.25 °C for proximal bipolar, 0.65 °C and 0.12 °C for distal bipolar, 1.10 °C and 0.30 °C for guarded quadripolar, and 1.78 °C and 0.36 °C for guarded tripolar configuration, respectively. *For each of these voltage-controlled simulations, the corresponding equivalent current is reported. [Color figure can be viewed at www.neuromodulationjournal.org]

Published by Elsevier Inc. on behalf of the International Neuromodulation Society.

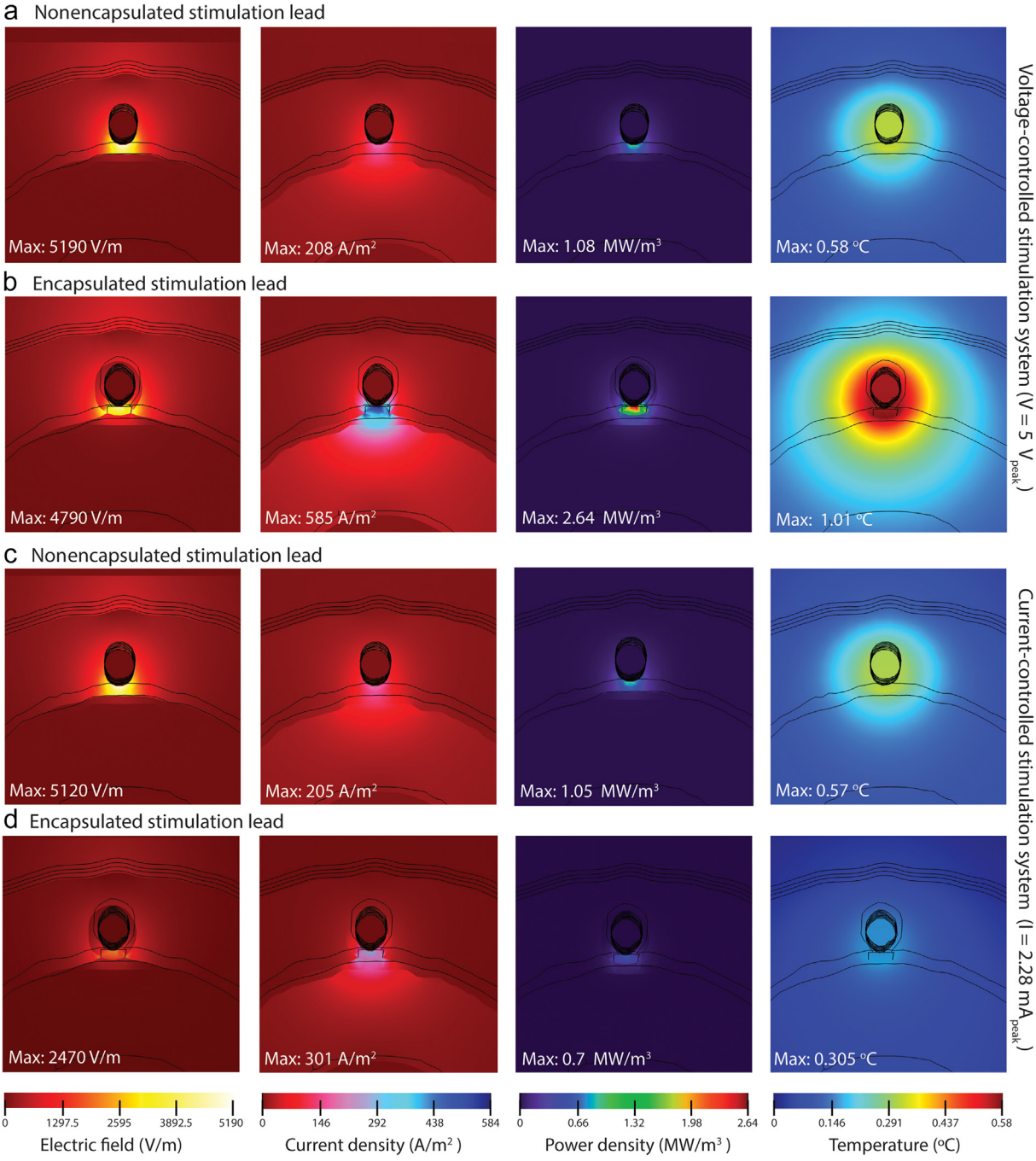

Figure 4. Systemic analysis of the impact of an encapsulation layer on voltage-controlled vs current-controlled SCS. We simulated the proximal bipolar HD SCS under voltage controlled (V = 5 V_{peak}) and current controlled with an applied current value matching that resulting in the voltage-controlled case with no encapsulation layer (I = 1.61 mA_{peak}). For voltage-controlled stimulation system (V = 5 V_{peak}), the maximum electric field, current density, power density, and temperature increase were respectively 5190 V/m, 208 A/m^2, 1.08 MW/m^3, and 0.58 °C for (a) the nonencapsulated lead condition and 4790 V/m, 585 A/m^2, 2.64 MW/m^3, and 1.01 °C for (b) the encapsulated lead condition. For the current-controlled stimulation system (I = 1.61 mA_{peak}), the maximum electric field, current density, power density, and temperature increase were respectively 5120 V/m, 205 A/m^2. 1.05 MW/m^3, and 0.569 °C for (c) the nonencapsulated lead condition and 2470 V/m, 301 A/m^2, 0.7 MW/m^3, and 0.305 °C for (d) the encapsulated lead condition. Max, maximum. [Color figure can be viewed at www.neuromodulationjournal.org]

density (from 208 A/m^2 to 585 A/m^2), resulting in an increase in power density (from 1.08 MW/m^2 to 2.64 MW/m^2) and so an increase in heating (from 0.59 °C to 1.01 °C). For current-controlled stimulation, the addition of an encapsulation layer halved the peak electric field (from 5120 V/m to 2470 V/m), and moderately increased the peak current density (from 205 A/m^2 to 301 A/m^2), resulting in a decrease in power density (from 1.05 MW/m^2 to 0.7 MW/m^2) and so a decrease in heating (from 0.57 °C to 0.30 °C).

DISCUSSION

HD SCS delivers increased energy (charge per second) by increasing duty cycle (frequency and/or pulse width).[2,7,8] We previously showed through phantom studies and computational modeling that 10-kHz SCS can increase tissue heating, directly reflecting its higher duty cycle.[8,9] HD SCS typically has a lower duty cycle than 10-kHz SCS, which—all things being equal—would result in less heating by HD SCS. Using FEM bioheat models (Fig. 1), in this study, we demonstrated the use of voltage-controlled stimulation (typical for HD SCS) results in different dependencies on encapsulation layer and electrode configuration vs current-controlled stimulation (used in conventional and 10-kHz SCS). As a result, under some clinically relevant stimulation conditions, HD SCS can produce spinal tissue heating greater than that of 10-kHz SCS (Fig. 2). For the first phase of this study, the voltage and current-controlled stimulation amplitudes chosen for comparison are not equal in magnitude but based on clinically relevant values. Similarly with our previous analysis of 10-kHz SCS,[31] our focus here is on heating as an ancillary mechanism of action for HD SCS pain control,[8] not as a safety concern, and predictions remain to be experimentally verified in situ.

The encapsulation layer (reflecting inflammatory response to the lead implantation and leading to scar tissue formation around the electrodes[12,23,32,33]) offers less resistance than epidural fat. Although current-controlled stimulation decreased heating with decreasing tissue resistivity, as presented by an encapsulation layer, voltage-controlled stimulation increased heating with decreasing tissue resistivity (Figs. 2 and 4). Under voltage-controlled stimulation, the use of more proximal leads and a tripolar electrode configuration reduced the effective interelectrode resistance, amplifying temperature increase (Fig. 3).

Tissue properties are complex and dynamic, which makes it intractable to simulate all thermo-electrical properties. Although validated in our previous works using in vitro phantoms,[8,9] our simulation results warrant in vivo or ex vivo measurements and validation. Given the importance of electrode design[8,15,17] and pulse shape[9,34] in heating, precise predictions warrant device-specific models.

Although the sensitivity of neuronal (eg, excitability and synaptic efficacy) and metabolic functions (eg, perfusion) to temperature has been studied experimentally,[7,30–32] the impact of potential heating on SCS outcomes remains to be determined.[8,9] In addition, for HD SCS (and other SCS approaches using a higher duty cycle and voltage control), our heating results suggest special consideration for alterations in electrode impedance, including reflecting vertebral level or distance from dural surface, changes over time with scar tissue buildup, (sudden) lead displacement, and patient postural changes.[29,35–39] To the extent heating is an ancillary mechanism of action, modeling pipelines developed previously[8,9] and applied in this study for the special cases of HD SCS and voltage-controlled SCS will inform programming under more divergent strategies than for conventional stimulation. For example, although electrode impedance is incidental in conventional SCS programming, for heating, it may be an explicit factor with, moreover, distinct implications for voltage vs current-controlled stimulation.

Authorship Statements

Adantchede L. Zannou, Niranjan Khadka, and Marom Bikson designed the study and prepared the manuscript with critically important inputs. Adantchede L. Zannou ran computer simulations, collected the data, and analyzed the data. Niranjan Khadka analyzed the data and edited the manuscript. Marom Bikson analyzed the data and edited the manuscript. All authors approved the final manuscript.

How to Cite This Article

Zannou A.L., Khadka N., Bikson M. 2022. Bioheat Model of Spinal Column Heating During High-Density Spinal Cord Stimulation.
Neuromodulation 2022; ■: 1–9.

REFERENCES

1. Wille F, Breel JS, Bakker EWP, Hollmann MW. Altering conventional to high density spinal cord stimulation: an energy dose-response relationship in neuropathic pain therapy. *Neuromodulation*. 2017;20:71–80. https://doi.org/10.1111/ner.12529.
2. Reddy CG, Dalm BD, Flouty OE, Gillies GT, Howard MA, Brennan TJ. Comparison of conventional and kilohertz frequency epidural stimulation in patients undergoing trialing for spinal cord stimulation: clinical considerations. *World Neurosurg*. 2016;88:586–591. https://doi.org/10.1016/j.wneu.2015.10.088.
3. High-density spinal cord stimulation for the treatment of pain in the rehabilitation patient. Anesthesia Key. Accessed October 31, 2021. https://aneskey.com/high-density-spinal-cord-stimulation-for-the-treatment-of-pain-in-the-rehabilitation-patient/
4. Miller JP, Eldabe S, Buchser E, Johanek LM, Guan Y, Linderoth B. Parameters of spinal cord stimulation and their role in electrical charge delivery: a review. *Neuromodulation*. 2016;19:373–384. https://doi.org/10.1111/ner.12438.
5. De Jaeger M, van Hooff RJ, Goudman L, et al. High-density in spinal cord stimulation: virtual expert registry (DISCOVER): study protocol for a prospective observational trial. *Anesth Pain Med*. 2017;7:e13640. https://doi.org/10.5812/aapm.13640.
6. Sweet J, Badjatiya A, Tan D, Miller J. Paresthesia-free high-density spinal cord stimulation for postlaminectomy syndrome in a prescreened population: a prospective case series. *Neuromodulation*. 2016;19:260–267. https://doi.org/10.1111/ner.12357.
7. Provenzano DA, Rebman J, Kuhel C, Trenz H, Kilgore J. The efficacy of high-density spinal cord stimulation among trial, implant, and conversion patients: a retrospective case series. *Neuromodulation*. 2017;20:654–660. https://doi.org/10.1111/ner.12612.
8. Zannou AL, Khadka N, Truong DQ, et al. Temperature increases by kilohertz frequency spinal cord stimulation. *Brain Stimul*. 2019;12:62–72. https://doi.org/10.1016/j.brs.2018.10.007.
9. Zannou AL, Khadka N, FallahRad M, Truong DQ, Kopell BH, Bikson M. Tissue temperature increases by a 10 kHz spinal cord stimulation system: phantom and bioheat model. *Neuromodulation*. 2021;24:1327–1335. https://doi.org/10.1111/ner.12980.
10. De Ridder D, Vanneste S, Plazier M, van der Loo E, Menovsky T. Burst spinal cord stimulation: toward paresthesia-free pain suppression. *Neurosurgery*. 2010;66:986–990. https://doi.org/10.1227/01.NEU.0000368153.44883.B3.
11. Al-Kaisy A, Van Buyten JP, Smet I, Palmisani S, Pang D, Smith T. Sustained effectiveness of 10 kHz high-frequency spinal cord stimulation for patients with chronic, low back pain: 24-month results of a prospective multicenter study. *Pain Med*. 2014;15:347–354. https://doi.org/10.1111/pme.12294.
12. Reynolds AF, Shetter AG. Scarring around cervical epidural stimulating electrode. *Neurosurgery*. 1983;13:63–65. https://doi.org/10.1227/00006123-198307000-00013.
13. Butson CR, Maks CB, McIntyre CC. Sources and effects of electrode impedance during deep brain stimulation. *Clin Neurophysiol*. 2006;117:447–454. https://doi.org/10.1016/j.clinph.2005.10.007.
14. Electromagnetics, Volume 2. Virginia Tech. Accessed February 8, 2022. https://vtechworks.lib.vt.edu/handle/10919/93253
15. Elwassif MM, Kong Q, Vazquez M, Bikson M. Bio-heat transfer model of deep brain stimulation induced temperature changes. *Conf Proc IEEE Eng Med Biol Soc*. 2006;2006:3580–3583. https://doi.org/10.1109/IEMBS.2006.259425.
16. Chang I. Finite element analysis of hepatic radiofrequency ablation probes using temperature-dependent electrical conductivity. *Biomed Eng OnLine*. 2003;2:12. https://doi.org/10.1186/1475-925X-2-12.
17. Elwassif MM, Datta A, Rahman A, Bikson M. Temperature control at DBS electrodes using a heat sink: experimentally validated FEM model of DBS lead architecture. *J Neural Eng*. 2012;9:046009. https://doi.org/10.1088/1741-2560/9/4/046009.

18. Pennes HH. Analysis of tissue and arterial blood temperatures in the resting human forearm. *J Appl Physiol*. 1948;1:93–122. https://doi.org/10.1152/jappl.1948.1.2.93.
19. Gabriel S, Lau RW, Gabriel C. The dielectric properties of biological tissues: II. Measurements in the frequency range 10 Hz to 20 GHz. *Phys Med Biol*. 1996;41:2251–2269. https://doi.org/10.1088/0031-9155/41/11/002.
20. IT'IS Foundation. Tissue Properties Database V3.0. https://itis.swiss/virtual-population/tissue-properties/downloads/database-v3-0/. Accessed February 8, 2021.
21. Mcintosh RL, Anderson V. A comprehensive tissue properties database provided for the thermal assessment of a human at rest. *Biophys Rev Lett*. 2010;05:129–151. https://doi.org/10.1142/S1793048010001184.
22. Grill W, Mortimer J. Electrical impedance of electrode encapsulation tissue. Paper presented at: 14th Annual International Conference of the IEEE Engineering in Medicine and Biology Society; October 29–November 1, 1992; Paris, France.
23. Grill WM, Mortimer JT. Electrical properties of implant encapsulation tissue. *Ann Biomed Eng*. 1994;22:23–33. https://doi.org/10.1007/BF02368219.
24. Sweet WH, Wepsic JG. Treatment of chronic pain by stimulation of fibers of primary afferent neuron. *Trans Am Neurol Assoc*. 1968;93:103–107.
25. Khadka N, Harmsen IE, Lozano AM, Bikson M. Bio-heat model of kilohertz-frequency deep brain stimulation increases brain tissue temperature. *Neuromodulation*. 2020;23:489–495. https://doi.org/10.1111/ner.13120.
26. Zander HJ, Graham RD, Anaya CJ, Lempka SF. Anatomical and technical factors affecting the neural response to epidural spinal cord stimulation. *J Neural Eng*. 2020;17:036019. https://doi.org/10.1088/1741-2552/ab8fc4.
27. Li S, Farber JP, Linderoth B, Chen J, Foreman RD. Spinal cord stimulation with 'conventional clinical' and higher frequencies on activity and responses of spinal neurons to noxious stimuli: an animal study. *Neuromodulation*. 2018;21:440–447. https://doi.org/10.1111/ner.12725.
28. Ahmed S, Yearwood T, De Ridder D, Vanneste S. Burst and high frequency stimulation: underlying mechanism of action. *Expert Rev Med Devices*. 2018;15:61–70. https://doi.org/10.1080/17434440.2018.1418662.
29. de Jongste MJ, Nagelkerke D, Hooyschuur CM, et al. Stimulation characteristics, complications, and efficacy of spinal cord stimulation systems in patients with refractory angina: a prospective feasibility study. *Pacing Clin Electrophysiol*. 1994;17:1751–1760. https://doi.org/10.1111/j.1540-8159.1994.tb03742.x.
30. Alò K, Varga C, Krames E, et al. Factors affecting impedance of percutaneous leads in spinal cord stimulation. *Neuromodulation*. 2006;9:128–135. https://doi.org/10.1111/j.1525-1403.2006.00050.x.
31. Khadka N, Bikson M. Response to the Letter to the Editor by Caraway et al. on "Tissue temperature increases by a 10 kHz spinal cord stimulation system: phantom and bioheat model". *Neuromodulation*. 2019;22:988. https://doi.org/10.1111/ner.13079.
32. Ranson M, Pope J, Deer T. Reducing Risks and Complications of Interventional Pain Procedures: Volume 5: A Volume in the Interventional and Neuromodulatory Techniques for Pain Management Series; Expert Consult Online and Print. Elsevier Health Sciences; 2012.
33. Jotwani R, Abd-Elsayed A, Villegas K, et al. Failure of SCS MR-conditional modes due to high impedance: a review of literature and case series. *Pain Ther*. 2021;10:729–737. https://doi.org/10.1007/s40122-020-00219-8.
34. Yearwood TL, Hershey B, Bradley K, Lee D. Pulse width programming in spinal cord stimulation: a clinical study. *Pain Phys*. 2010;13:321–335.
35. Taccola G, Barber S, Horner PJ, Bazo HAC, Sayenko D. Complications of epidural spinal stimulation: lessons from the past and alternatives for the future. *Spinal Cord*. 2020;58:1049–1059. https://doi.org/10.1038/s41393-020-0505-8.
36. Abejón D, Rueda P, Vallejo R. Threshold evolution as an analysis of the different pulse frequencies in rechargeable systems for spinal cord stimulation. *Neuromodulation*. 2016;19:276–282. https://doi.org/10.1111/ner.12401.
37. Cameron T, Alo KM. Effects of posture on stimulation parameters in spinal cord stimulation. *Neuromodulation*. 1998;1:177–183. https://doi.org/10.1111/j.1525-1403.1998.tb00014.x.
38. Olin JC, Kidd DH, North RB. Postural changes in spinal cord stimulation perceptual thresholds. *Neuromodulation*. 1998;1:171–175. https://doi.org/10.1111/j.1525-1403.1998.tb00013.x.
39. Lempka SF, Johnson MD, Miocinovic S, Vitek JL, McIntyre CC. Current-controlled deep brain stimulation reduces in vivo voltage fluctuations observed during voltage-controlled stimulation. *Clin Neurophysiol*. 2010;121:2128–2133. https://doi.org/10.1016/j.clinph.2010.04.026.